



ARTICLE

<https://doi.org/10.1038/s41467-019-08553-y>

OPEN

Emergence of the structure-directing role of f-orbital overlap-driven covalency

Erli Lu¹, Saira Sajjad^{1,2}, Victoria E.J. Berryman¹, Ashley J. Wooles¹,
Nikolas Kaltsoyannis ¹ & Stephen T. Liddle ¹

FEUDAL (f's essentially unaffected, d's accommodate ligands) is a longstanding bonding model in actinide chemistry, in which metal-ligand binding uses 6d-orbitals, with the 5f remaining non-bonding. The inverse-trans-influence (ITI) is a case where the model may break down, and it has been suggested that ionic and covalent effects work synergistically in the ITI. Here, we report an experimentally grounded computational study that quantitatively explores the ITI, and in particular the structure-directing role of f-orbital covalency. Strong donor ligands generate a *cis*-ligand-directing electrostatic potential (ESP) at the metal centre. When f-orbital participation, via overlap-driven covalency, becomes dominant via short actinide-element distances, this ionic ESP effect is overcome, favouring a *trans*-ligand-directed geometry. This study contradicts the accepted ITI paradigm in that here ionic and covalent effects work against each other, and suggests a clearly non-FEUDAL, structure-directing role for the f-orbitals.

¹School of Chemistry, The University of Manchester, Oxford Road, Manchester M13 9PL, UK. ²Department of Chemistry, COMSATS Institute of Information Technology, Abbottabad, 22060 Abbottabad, Pakistan. These authors contributed equally: Erli Lu, Saira Sajjad, Victoria E.J. Berryman. Correspondence and requests for materials should be addressed to N.K. (email: nikolas.kaltsoyannis@manchester.ac.uk) or to S.T.L. (email: steve.liddle@manchester.ac.uk)

One of the most fascinating, enduring, and controversial topics in molecular actinide science is the continuously debated nature and extent of the chemical bonding of the early members of the series, and in particular uranium, and how this relates to structure and periodic trends within the context of the entire Periodic Table^{1–19}. The role of s-, p-, and d-orbitals in chemical bonding and how this relates to the geometries of main group and transition metal complexes is now well understood. For lanthanides, the bonding is usually described as overwhelmingly ionic and non-directional with little orbital contribution; however, where covalency is invoked, for example where the *trans*-influence (TI) has been observed^{20–30}, it is usually d-orbitals that are involved^{27,31,32}. By contrast, for the early actinides there is still debate over the extent and tensioning of f- vs d-orbital character^{7,8,14} and, given that electrostatics are generally accepted as the dominant feature of the bonding, the structure directing role of the 5f-orbitals remains a moot point³³.

A longstanding conceptual bonding model in actinide chemistry is Bursten's FEUDAL (f's essentially unaffected, d's accommodate ligands). This model advances the notion that actinides bind primarily using their d-orbitals and the f-orbitals remain mainly non-bonding^{34,35}. This view seems to hold for ions like uranium when bonded to expansive ligands that have low angular requirements, e.g. C₅-8-arenes^{36–41}, but in recent years this has been increasingly challenged when small ligands with more acute angular requirements, e.g. nitrides, are considered^{42,43}. However, although this model considers the issue of orbital interactions it does not directly address whether f-orbitals are structure directing, but their characterisation as 'unaffected' implicitly suggests no structure-directing role. Moreover, there are hints in the literature that FEUDAL sometimes breaks down in scenarios where structure-directing effects involving f-orbitals are invoked. The longstanding, preeminent example of this is the inverse-*trans*-influence (ITI)^{44–46}, where strongly donating ligands are preferentially found to be *trans* to one another. The most prevalent example of this is uranyl; e.g. in [UO₂Cl₂(OPPh₃)₂] the two oxos are mutually *trans* in direct contrast to [MoO₂Cl₂(OPPh₃)₂] where they are *cis*^{47–50}. In recent years a variety of non-uranyl complexes that seem to exhibit the ITI have been reported, usually with uranium in oxidation states V and VI and with nitride or oxo ligands^{43,51–56}. Two hypotheses have been developed to account for the ITI^{45,46,57–59}. From an orbital perspective, it is proposed that the 6p-orbitals of early actinides are semi-core, and therefore semi-valence, and can donate electron density into vacant 5f-orbitals; thus, an electron hole forms that is compensated by increased electron donation from a *trans* ligand. Alternatively, a polarisation argument can be employed; when the parity of overlapping orbitals is *u-g*, as is the case with p-d orbitals, a dipolar arrangement at the metal disfavours *trans* and stabilises *cis* positions, whereas when the parity is the same, e.g. *u-u* for p-f orbitals, then the charge distribution is quadrupolar with *trans* favoured and *cis* disfavoured. It should be noted that these working theories are based on logical, but suppositional, arguments, and although the majority of studies have focussed on establishing the role of the 6p- and/or 5f-orbitals, their precise roles remain somewhat nebulous. Furthermore, although the traditional view of the ITI is that ionic and covalent effects compete with one another, it has been suggested that this is misleading³³, and that ionic and covalent effects are actually working together synergistically.

At this point, a clarification of the term covalency is merited^{60–62}. Covalency, that is the mixing coefficient, is proportional to the spatial overlap of the orbitals divided by the difference in their energies, and these two parameters are independent of one another^{7,8}. So, covalency can increase by increased spatial overlap or by reduction in the difference of parent atomic orbital energies.

The latter, which is called near-energy driven covalency, is a perfectly valid definition of covalency when framed in context, but chemical bonding carries the connotation of orbital overlap resulting in electron density building up in the inter-nuclear region. The former is called overlap-driven covalency, and it is on this aspect that discussions in this paper will focus.

We recently reported, Fig. 1, an extension of the ITI to tetra-valent cerium, uranium, and thorium *trans bis*(carbene) complexes (1Ce, 1U, 1Th)⁶² and latterly found that in carbene-imido derivatives of uranium, *cis* geometries were overwhelmingly favoured (2UNHRK and 2UBIPY)^{63,64}. It is important to note that in the former the *trans* disposition is enforced by ligand steric constraints yet the *trans* carbenes are strongly bound to the metals with short M=C bond distances, but in the latter even when steric constraints are removed the *cis* geometry dominates. Since uranium often uses more 5f- than 6d-orbital character in its bonding, but the reverse is usually found for thorium, we prepared analogous thorium carbene-imido complexes. Again, a *cis* geometry is preferred, which spurred us to survey the inherent *cis* or *trans* preferences for carbene-carbene, carbene-imido, and carbene-oxo ligand combinations for cerium, uranium, and thorium. Though many systems indeed prefer *cis* geometries, we notably find that the cerium and uranium oxo systems go against this trend and in fact prefer *trans* geometries. This study puts the original proposition of the ITI on a quantified, firm footing and reveals that the electrostatic potential (ESP) surface around the metal centre directs the *cis* geometries. This first concerted application of ESP arguments to this issue reveals that d-orbital participation is in fact not the driving force for *cis* geometries, but opportunistically results from ESPs. When f-orbital participation, and associated overlap-driven covalency, becomes dominant, the ionic effect is overcome and a *trans* geometry is favoured. This study therefore demonstrates that ionic and covalent effects work against each other in cases where the structure-directing role of f-orbitals is confirmed, the latter aspect challenging the generality of the FEUDAL model.

Results

Synthesis, characterisation, and solid state structures. With 1M (M = Ce, U, Th) and 2UNHRK and 2UBIPY reported^{62–64}, we sought to prepare the analogous R₂C = Th^{IV} = NCPH₃ (2Th, R = Ph₂PNSiMe₃) complexes, in order to now map out the TI/ITI structural influences across the C = M^{IV} = E (E = CR₂, NCPH₃) series, Fig. 2. It is noteworthy that in comparison with the burgeoning nature of uranium-ligand multiple bond species^{3,6,12–14}, thorium-ligand multiple bond species are less developed. Indeed, for thorium 2-metalla-allenes, despite their significant importance as relatives of ThO₂, two homoleptic thorium-*bis*(carbenes) are the only such species in the literature^{62,65} and there are no heteroleptic thorium-2-metalla-allenes. The previously reported thorium-carbene-*bis*(alkyl) [Th^{IV}(BIPM^{TMS})(CH₂SiMe₃)₂] (3)⁶², which has a pre-installed Th=C double bond interaction, was found to be a suitable precursor to preparing C = Th^{IV} = N linkages, Fig. 2 (see Supplementary Information). Complex 3 is straightforwardly converted, via the diamide (4) or alkyl-amide (5) into 2ThBIPY or 2ThNHRK, respectively, which bear the desired C = Th^{IV} = N unit, via two-step syntheses that involve deprotonations facilitated by external (for 2ThNHRK) or internal (for 2ThBIPY) Brønsted bases, and these complexes are isolated as red crystalline solids in satisfactory yields. The formulations of 2ThNHRK and 2ThBIPY are supported by NMR, IR, and optical spectroscopies, and elemental analyses (see Supplementary Figures 1 to 14).

Beyond the spectroscopic data, the structures of 2ThNHRK and 2ThBIPY are unambiguously confirmed by X-ray single

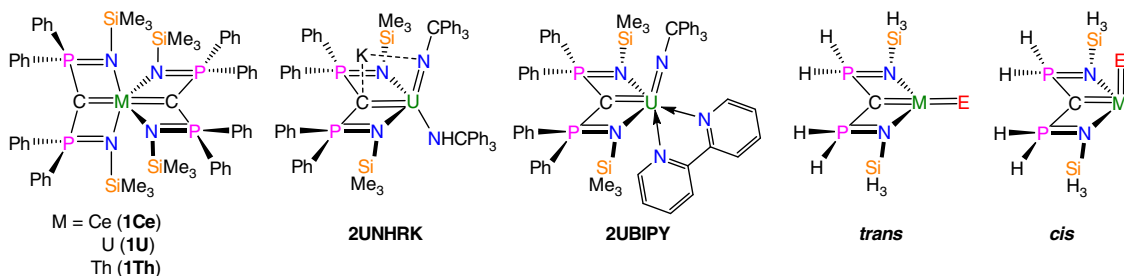


Fig. 1 Carbene complexes. Previously reported work^{63,64} and *trans* and *cis* models studied in this work

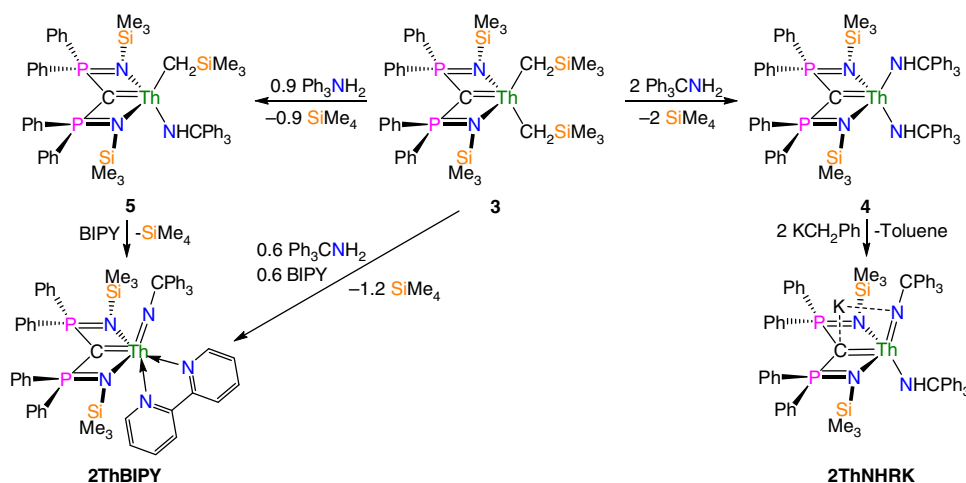


Fig. 2 Synthesis of complexes **2ThBIPY** and **2ThNHRK**. The known dialkyl complex **3** can be reacted two equivalents of trityl-amine by protonolysis to give the diamide complex **4**. Complex **4** when treated with two equivalent of benzyl potassium (to maximise the yield, a stoichiometric amount of benzyl potassium gives lower yields) converts to the amide-imide complex **2ThNHRK**. Complex **3** can alternatively be reacted with a sub-stoichiometric quantity of trityl-amine (to suppress ligand-redistribution reactions) to give, via protonolysis, the mixed alkyl-amide complex **5**. Complex **5** undergoes α -hydrogen abstraction on addition of BIPY to give **2ThBIPY**

crystal diffraction, Fig. 3. The salient structural feature of these complexes is the *cis*-C=Th^{IV}=N units [C=Th=N for **2ThNHRK** and **2ThBIPY** = 107.08(19) and 110.90(9)°, respectively], which is similar to **2U** analogues, suggesting the presence of a TI. Structurally speaking, though a potassium ion is intimately coordinated in the structure of **2ThNHRK** the Th=N_{imide} and Th=C_{carbene} bonds in this complex are little disturbed from what might be anticipated for formal thorium-nitrogen and -carbon double bond interactions [Th=N_{imide} for **2ThNHRK** and **2ThBIPY** = 2.109(5) and 2.067(2) Å; Th=C_{carbene} for **2ThNHRK** and **2ThBIPY** = 2.564(6) and 2.558(3) Å, respectively]. The Th-N_{BIPY}, C-N and C-C bond lengths in the bipyridine fragment of **2ThBIPY** are consistent only with a neutrally coordinated BIPY ligand⁶⁶.

Computational geometry optimisations. Building on our previous study of **2UBIPY**⁶⁴, we investigated a family of nine metalla-allene model systems [C]=M=E ([C]=C (PH₂NSiH₃)₂; M = Ce^{IV}, Th^{IV}, U^{IV}; E = C(CH₃)₂, NCH₃, O), with a particular focus on the C-M-E angle, using the Gaussian-09 code⁶⁷ with two density functional approximations (DFAs). We used the generalised gradient approximation (GGA), PBE^{68,69}, and related hybrid, PBE0⁷⁰; these DFAs are ideal as PBE has recently been shown to give accurate geometries in an extensive benchmarking study of organouranium systems⁷¹, and the GGA BP86 performs better than B3LYP and certain Minnesota functionals for some uranium bis carbene complexes⁷², and PBE0 is known to give improved energetics and has been

previously applied by us to the study of a uranium(IV)-carbene-imido complexes^{63,64}. Model complexes were sterically truncated and void of potassium ions and co-ligands to isolate electronic effects from steric constraints, and the final equilibrium geometries are obtained irrespective of whether the starting geometry is *cis* or *trans* with respect to the [C]=M=E angle. The results are collected in Supplementary Tables 1 to 5, from which it can be seen that there is little difference between the two DFAs. All the systems with E = C(CH₃)₂ and NCH₃ adopt a *cis* geometry. However, for the oxo complexes only [C]=Th=O has a *cis* conformation (C-Th-O angle = 116.8/116.6°), whereas [C]=Ce=O and [C]=U=O prefer *trans* geometries, with C-M-O angles of 165.1/162.2° and 176.9/176.4°, respectively, at the PBE0/PBE level.

Computational total energy surface scans. To further probe the energetic preference for *cis* or *trans* conformations, total self-consistent field (SCF) energy surfaces were explored as a function of the C-M-E angle, as defined by the *trans* and *cis* models on the right-hand side of Chart 1. All geometric parameters were relaxed except this angle, which was perturbed in 5° increments from the optimised geometry. The resulting plots for the E=C(CH₃)₂, NCH₃ and O systems are shown in Fig. 4a–c, respectively. The data for [C]=M=C(CH₃)₂ and [C]=M=NCH₃ are similar to one another; in both cases the Th molecule has the largest preference for a *cis* geometry, followed by U and then Ce, which are similar. We have attempted to quantify these preferences by locating transition states (TSs), starting from the highest points of the SCF

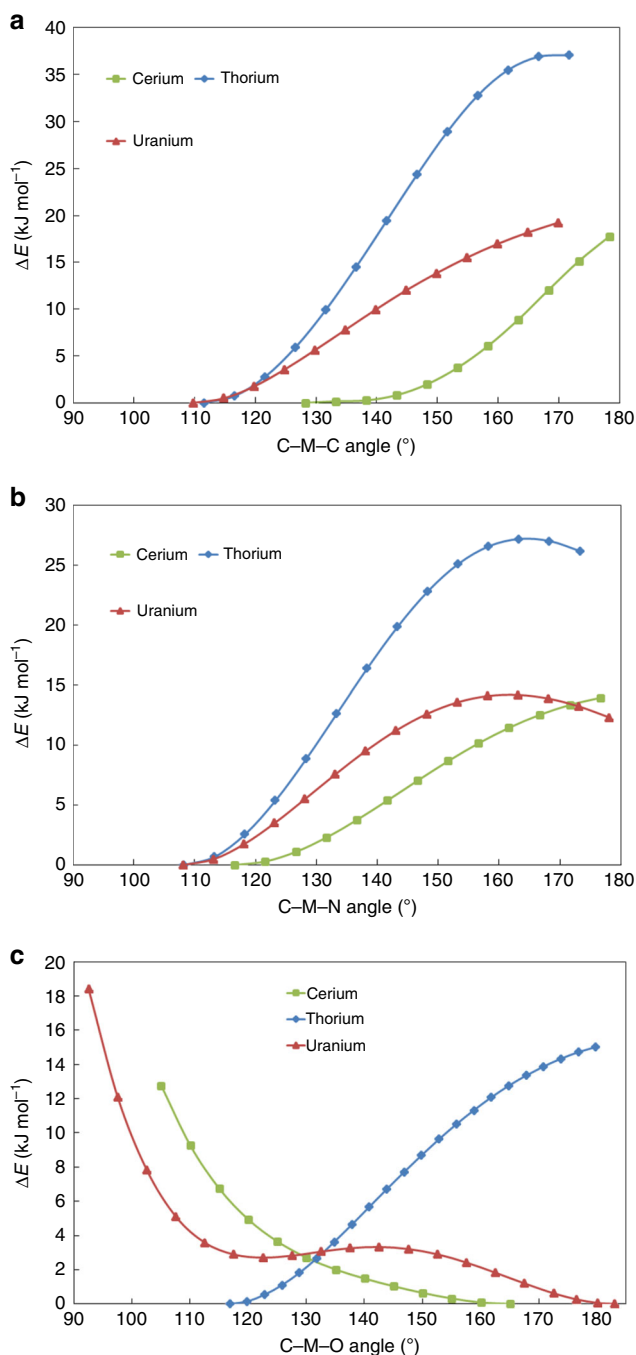


Fig. 4 PBE0 SCF energy surface scans of $[C]=M=E$ angles, $M=Ce, Th, U$. **a** $E=C(CH_3)_2$, **b** $E=NCH_3$, **c** $E=O$. Energies (kJ mol⁻¹) are presented relative to those of the fully optimised structures

to the M-E σ -bonding NLMO against the $[C]=M=E$ angle for all nine targets; there is a striking correlation, with $R^2 = 0.88$ at the PBE0 level, indicating that the larger the total f-orbital contribution to the σ -bonding NLMO the larger the $[C]=M=E$ angle, i.e. the $[C]=M=E$ angle is a function of f-orbital based overlap-driven covalency. In contrast, there is very little correlation of the $[C]=M=E$ angle with metal d-character to the NLMO σ -bonding ($R^2 = 0.36$ at the PBE0 level).

If indeed the interaction of the (model) BIPM ligand with the metal centre directs the E ligand into the *cis* position due to the asymmetric ESP, it would be expected that reducing that interaction by moving the [C] away from the metal would

reduce the effect. We therefore moved the model BIPM ligand away from the metal centre by extending the distance between the metal and the central C atom of [C] by 1 Å, and probed the effect on the energy barrier to alteration of the C-M-E angle. As expected, these barriers are either reduced significantly or removed altogether; the effect on the $[C]=Th=C(CH_3)_2$ system is shown in Supplementary Figure 16. For this molecule, the barrier is reduced by more than half. Extending this argument, elongating the M-O distance in either $[C]=Ce=O$ or $[C]=U=O$ should reduce the M-O interaction and favour a smaller C-M-O angle. This was probed by lengthening the Ce-O distance from its optimised value of 1.77 to 3.0 Å, and indeed the preferred C-Ce-O angle decreases from 165 to 135°.

For all seven C-M-E bending TSs located (Supplementary Table 4), there is very little change in $r(M-E)$, but in all cases bar $[C]=U=O$ there is significant elongation (>0.08 Å) of $r(M-C_{[C]})$ at the TS. This lengthening, and presumably weakening, of the M-C_[C] interaction destabilises the TS vs the true minimum geometry. By contrast, the changes in both $r(M-E)$ and $r(M-C_{[C]})$ at the bending TS located for $[C]=U=O$ are very modest, in agreement with this TS being of much lower relative energy than the other six. Indeed, the energy surfaces presented in Fig. 4a–c suggest that the TS for $[C]=U=O$ could be considered separately from the rest.

The classic *trans* influence in transition metal element chemistry arises from the competition for metal d-orbitals between two mutually *trans* ligands, resulting in the elongation of the bond *trans* to the stronger donor ligand. If this were a key factor in our systems, we would expect the lengthening of $r(M-C_{[C]})$ to be related to the d-orbital content of the M-E NLMO at the TS. However, we find essentially no such correlation between these variables; $R^2 = 0.20$ for the correlation of the total metal d-orbital contribution to the TS' M-E σ NLMO with the $r(M-C_{[C]})$ elongation (in the six TSs bar that in $[C]=U=O$). An alternative explanation for the $r(M-C_{[C]})$ elongation is an extension of the electrostatic argument presented above; rotating the E ligands away from the optimised C-M-E angles and towards linearity moves them from the orientation favoured by the asymmetric ESP surface around the metal, and the system adjusts by attempting to reduce the asymmetric ESP by elongating $r(M-C_{[C]})$.

GGA-type DFAs typically favour greater electron delocalisation, leading to more radially diffuse orbitals. It is interesting to note that for almost all of the complexes studied here the GGA-type functional, PBE, produces σ -bonding NLMOs with greater f-orbital character (Table 1). The only exception is $[C]=U=NCH_3$, which shows a significant increase in s orbital contribution. However, it is important to note that the differences between PBE and PBE0 are slight, and a consistent trend emerges whereby the f-orbital contribution is, like-for-like, always greater than the d-orbital contribution for Ce and U compared to Th. This is the case irrespective of the identity of E, but is certainly most pronounced for the oxo complexes, giving confidence that the high f-orbital contributions to the Ce=O and U=O bonds are real and not a computational artefact.

Topological bonding analysis. To further investigate the bonding between the metal centre and E ligand, analysis of the topology of the electron density was carried out with the Quantum Theory of Atoms in Molecules (QTAIM)^{74,75}. We focus on three parameters; the electron density at the bond critical point (BCP) along the bond path between the M and C/N/O atomic centres (ρ_{BCP}), the total energy density at the BCP (H_{BCP}) and the delocalisation index between the M and C/N/O atomic basins $\delta(M,E)$. The magnitudes of these parameters, in an absolute sense,

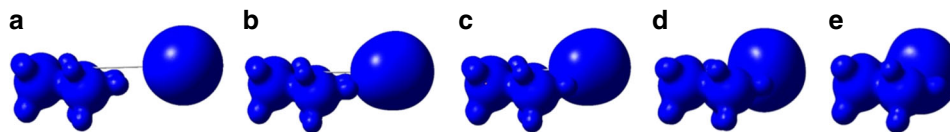


Fig. 5 Electrostatic potential (ESP) surface of the $[C]=Th^{2+}$ fragment. As a function of distance this shows the approach of the model BIPM $[C]$ ligand to the Th $[r(Th-C_{[C]})]$ at **a** 6.491 Å, **b** 5.491 Å, **c** 4.491 Å, **d** 3.491 Å, **e** 2.491 Å, the value in the optimised structure of $[C]=Th=NCH_3$. The isovalue is 0.5

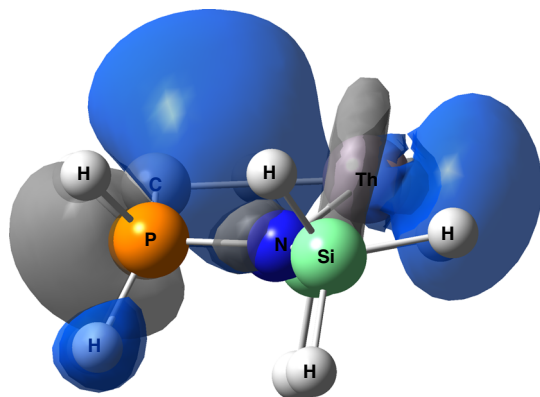


Fig. 6 NLMO of $[C]=Th^{2+}$. This NLMO has significant amplitude in the *trans* direction, resulting in a *cis* directing effect. The orbital is 16.86% Th character, and that component is composed of 19.77% 7s, 63.88% 6d, and 16.05% 5f

provide a measure of the overall extent of covalency in the bonding interactions. The data for the nine model complexes are summarised in Table 2, and reveal some clear trends. For a given metal, all three metrics increase (in an absolute sense) in the order $C(CH_3)_2 < NCH_3 < O$ while, for a given E ligand, the QTAIM metrics increase in the order $Th < U < Ce$. The data indicate that $[C]=Ce=O$ and $[C]=U=O$ have the most covalent M-E interactions, in agreement with the suggestion that the *cis*-directing ESP is overcome only in the most covalent of our systems.

The QTAIM metrics give us a measure of overall covalency, whereas NLMO analysis allows us to assess specific orbitals. Together they provide complementary methods to assess covalency and, ideally, we expect correlations between the data from the two techniques. This is assessed in Table 3, where the regression analyses for the correlation of a number of key variables are presented. In all but three cases, the R^2 values are well over 0.9, indicating strong correlations between the NLMO and QTAIM metrics. This is particularly so for ρ_{BCP} . That both orbital and electron density-based assessments of covalency correlate so well gives confidence in our conclusions regarding the extent of covalency in these An-E interactions.

Discussion

Noting the orbital and parity arguments for the ITI presented above, we recognise that either of these logical, but largely speculative, arguments can be combined and subsumed into the ESP argument based on the calculation on the electronic structure of $[[C]=M]^{2+}$. It is clear from the computed data that the thorium complexes have much the strongest preference for a *cis* geometry. At first, if considering orbital arguments, this is counterintuitive because the bonding of thorium is more ionic than uranium and so orbital factors, and thus the *cis* effect, should be diminished.

However, when an ESP argument is considered, the stronger preference of thorium to adopt a *cis* geometry falls entirely into line with what would be predicted based on where the charge build-up occurs, i.e. *trans*, thus leaving a *cis* hole to accommodate a *cis* ligand. This might be linked to thorium d-orbital character, however although the computed data in Table 1 superficially supports this, more detailed assessment shows that this is not the case. This leads us to an important conclusion, which is that in the absence of other drivers it is the ESP that dominates the resulting geometry; this is not contingent on the d-orbital character in the M-E bond, but this does not mean that d-orbitals may not be used as a consequence. So, d-orbital character may result from the *cis* geometry but the *cis* geometry does not itself result from d-orbital character. This ESP argument thus extends and refines Denning's original proposition^{45,46} into a more quantified, and firmer, basis.

Having established that the preferred geometry of the complexes in this study is *cis*, we now address why $[C]=U=O$ and $[C]=Ce=O$ prefer *trans* geometries. We propose that the optimised $[C]=M=E$ angles arise from the interplay of electrostatic (ionic) and orbital (covalent) effects; the former favour the *cis* orientation while the latter favour linearity. It is likely that the orbital effects dominate in $[C]=Ce=O$ and $[C]=U=O$ because of the small size of O^{2-} ; these two systems have the shortest M-E distances (Supplementary Table 4) and hence only in $[C]=Ce=O$ and $[C]=U=O$ is the M-E distance short enough to allow sufficient f-orbital/ligand overlap for the covalent driver to linearity to overcome the *cis*-directing ionic effect. Certainly, f-character dominates the M-E σ -bonding NLMOs of $[C]=U=O$ and $[C]=Ce=O$ in contrast to the other seven model systems where d-character dominates, Table 1. Looking more widely, it is certainly the case that where the ITI clearly occurs or is proposed to occur this almost always involves small, highly charged ligands such as N^{3-} and O^{2-} with short M-E distances^{43,51-57}. In other words, given the radially contracted nature of 5f orbitals compared to 6d, only at short M-E distances can the 5f-orbitals come into the bonding picture and exert their influence to favour a *trans* $[C]=M=O$ geometry. As we noted earlier, the oxo systems require significantly smaller energies to manipulate the C-M-E angle in comparison with the C- and N-based systems, and we suggest that this is because the ionic and covalent effects are most finely balanced in these molecules. For $E=C(CH_3)_2$ and NCH_3 , Th has much the strongest preference for the *cis* geometry, and $[C]=Th=O$ is the only oxo to favour significantly bent C-Th-O. For a given E ligand, the Th compound has the lowest f contribution to the M-E σ -bonding NLMO, and the QTAIM metrics are the smallest. Hence the Th-E interaction is clearly the most ionic and its geometry is dominated by electrostatics. By contrast, for $[C]=M=O$ (M=Ce, U) f-orbital covalency plays a structure-dictating role, something normally (i.e. in the FEUDAL model) limited to d-orbitals. Indeed, even for lanthanides ITI effects have been convincingly attributed to the role of d-, not f-, orbitals in bonding to ligands^{27,31}. We therefore suggest that, within the interplay of early actinide ionic vs covalent effects, the structure-directing capacity of overlap-driven covalency is not solely the domain of the d-orbitals.

Table 1 Composition (%) of the M-E σ bonding NLMOs of [C]=M=E ([C]=C(PH₂NSiH₃)₂; M=Ce, Th, U; E=C(CH₃)₂, NCH₃, O) at their optimised geometries^a

E	M	Functional	Contribution of M to the σ -bonding NLMO					Total d	Total f
			M	s	p	d	f		
C(CH ₃) ₂	Ce	PBE0	31.19	1.48	0.09	63.74	34.66	19.88	10.81
		PBE	30.41	2.84	0.09	60.05	37.00	18.26	11.25
	Th	PBE0	23.09	7.19	0.44	78.05	14.31	18.02	3.30
		PBE	24.17	8.29	0.47	75.73	15.50	18.30	3.75
	U	PBE0	28.89	8.32	0.24	61.19	30.25	17.68	8.74
		PBE	30.56	10.59	0.21	56.83	32.36	17.37	9.89
NCH ₃	Ce	PBE0	19.58	3.75	0.14	69.97	26.13	13.70	5.12
		PBE	18.61	4.65	0.17	67.37	27.80	12.54	5.17
	Th	PBE0	15.36	6.57	0.95	75.09	17.35	11.53	2.66
		PBE	15.86	7.13	1.07	73.30	18.48	11.63	2.93
	U	PBE0	19.18	7.91	0.28	60.01	31.77	11.51	6.09
		PBE	19.67	11.25	0.32	59.94	28.48	11.79	5.60
O	Ce	PBE0	26.60	3.04	0.38	32.90	63.53	8.75	16.90
		PBE	26.47	3.02	0.45	31.33	65.14	8.29	17.24
	Th	PBE0	16.11	1.48	4.92	59.70	33.77	9.62	5.44
		PBE	16.80	1.73	5.32	56.38	36.49	9.47	6.13
	U	PBE0	24.20	1.73	0.59	22.84	74.79	5.53	18.10
		PBE	23.94	1.42	0.58	22.44	75.52	5.37	18.08

^aThe total d and total f values are the products of the metal contribution and its d and f breakdowns

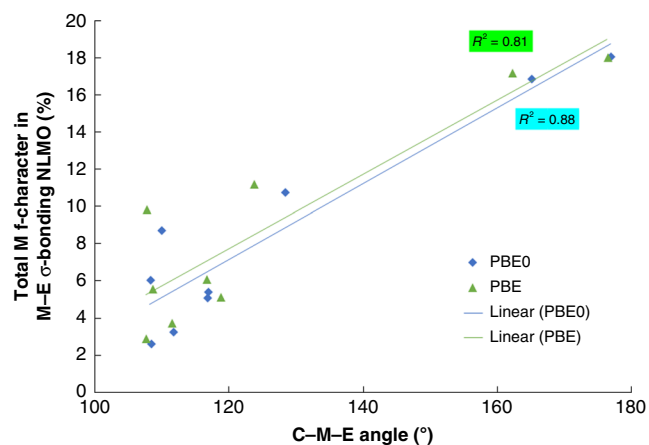


Fig. 7 The C-M-E angle (°) vs the total metal f character in the M-E σ bonding NLMO (%) of [C]=M=E. C=C(PH₂NSiH₃)₂; M=Ce, Th, U; E=C(CH₃)₂, NCH₃, O). R² with PBE0 (PBE) for Ce, Th, and U are 0.93 (0.83), 0.97 (0.96), and 0.96 (0.88), respectively

To summarise, we have prepared thorium-carbene-imido complexes, which together with uranium analogues has enabled us to conduct an experimentally grounded computational study into TI and ITI effects in carbene-carbene, carbene-imido, and carbene-oxo ligand combinations at uranium, thorium, and cerium. By conducting calculations on models freed from steric and counter-ion constraints, we have been able to place the ITI on a quantified, firmer footing. We find that a strong donor ligand such as the carbene generates an ESP that is inherently *cis*-directing in terms of subsequent ligand coordination. This reveals that d-orbital participation in the M-E bonds may opportunistically result from this ESP but does not drive it. When f-orbital participation, with associated overlap-driven covalency, becomes dominant via short M-E distances then this ionic effect is overcome and a *trans* geometry is favoured. This study therefore contradicts the previous assessment of the ITI as resulting from

Table 2 QTAIM properties (PBE0) for the M-E interaction in [C]=M=E ([C]=C(PH₂NSiH₃)₂; M=Ce, Th, U; E=C(CH₃)₂, NCH₃, O)^a

E	M	ρ_{BCP}	H_{BCP}	$\delta(\text{M,E})$
C(CH ₃) ₂	Ce	0.166	-0.093	1.56
	Th	0.146	-0.078	1.39
	U	0.156	-0.082	1.48
NCH ₃	Ce	0.195	-0.123	1.89
	Th	0.178	-0.110	1.63
	U	0.197	-0.125	1.80
O	Ce	0.284	-0.247	1.91
	Th	0.242	-0.202	1.68
	U	0.278	-0.242	1.87

^a ρ_{BCP} is the bond critical point between the M and C/N/O centres, H_{BCP} is the total energy density at that bond critical point, and $\delta(\text{M,E})$ is the delocalisation index between the M and C/N/O atomic basins

synergistic interplay of ionic and covalent effects in that here the data suggest that they work against each other in cases where the structure-directing role of f-orbitals is confirmed. This work therefore also suggests an instance where FEUDAL breaks down. The structure-directing capacity of overlap-driven covalency would therefore seem to be not solely the domain of the d-orbitals; here the suggestion of the structure-directing role of f-orbital overlap-driven covalency emerges.

Methods

Preparation of [Th{C(PPh₂NSiMe₃)₂}(NH₂CHPh₃)₂] (4). At -78 °C, a solution of Ph₃CNH₂ (0.830 g, 3.2 mmol) in toluene (10 ml) was added to a stirring solution of **3** (1.926 g, 2 mmol) in toluene (10 ml). The mixture was allowed to stir at -78 °C for 30 min and at ambient temperature for 3 h. After which, the mixture was filtered, and all volatiles in the filtrate were evaporated under vacuum to afford a viscous yellow oil. The oil was washed with pentane (5 ml × 4) and dried under vacuum to afford **4** as a yellow solid. Yield: 1.400 g, 54%. Single crystals suitable for X-ray diffraction were obtained from toluene solution at 0 °C. Anal. Calcd for C₆₉H₇₀N₄P₂Si₂Th·0.5(C₇H₈): C, 64.43; H, 5.52; N, 4.15. Found: C, 63.64; H, 5.60; N, 3.64. ¹H NMR (C₆D₆, 298 K): δ (ppm) 0.01 (s, 18 H, -SiMe₃), 4.03 (s, 2 H, -NHCPh₃), 6.95–6.99 (m, 9 H, ArH), 7.02–7.08 (m, 13 H, ArH), 7.18–7.20 (m, 9 H,

Table 3 Correlation (R^2) between QTAIM and NLMO properties (PBE0) of the M-E interaction in $[C]_2M-E ([C]_2=C(PH_2NSiH_3)_2; M=Ce, Th, U; E=C(CH_3)_2, NCH_3, O)^a$

Variables		R^2		
		$C(CH_3)_2$	NCH_3	O
Total M character in σ bonding M-E NLMO (%)	vs ρ_{BCP}	0.941	0.967	0.950
	vs H_{BCP}	0.773	0.956	0.943
	vs $\delta(M,E)$	0.956	0.933	0.918
Total M f orbital character in σ bonding M-E NLMO (%)	vs ρ_{BCP}	0.937	0.967	0.953
	vs H_{BCP}	0.766	0.976	0.965
	vs $\delta(M,E)$	0.953	0.657	0.939

^a ρ_{BCP} is the bond critical point between the M and C/N/O centres, H_{BCP} is the total energy density at that bond critical point, and $\delta(M,E)$ is the delocalisation index between the M and C/N/O atomic basins

ArH), 7.54–7.59 (m, 19 H, ArH). ³¹P NMR (C₆D₆, 298 K): δ (ppm) 4.70 (s). ¹³C {¹H} NMR (C₆D₆, 298 K): δ (ppm) 3.91 (s, -SiMe₃), 77.81 (s, -NHCPh₃), 126.90, 128.78, 129.00, 129.46, 130.10 (ArC), 131.69 (t, ²J_{PC} = 5.0 Hz, C_{meta} of P-Ph), 139.72 (t, ¹J_{PC} = 49.1 Hz, C_{ipso} of P-Ph), 152.20 (ArC). ATR-IR ν cm⁻¹: 3052 (w), 3019 (w), 2947 (w), 2892 (w), 1594 (w), 1488 (m), 1435 (s), 1346 (s), 1282(s), 1246 (m), 1177 (s), 1149 (m), 1105 (m), 1080 (s), 1043 (m), 1024 (s), 831 (m), 764 (m), 695 (s), 637 (s), 603 (m), 545 (m), 526 (s), 509 (s), 471 (s), 457 (s), 410 (s).

Preparation of [Th{C(PPh₂NSiMe₃)₂}(=NCPPh₃)(-NHCPh₃)(K) (2ThNHRK). At ambient temperature, 15 ml of benzene was added to a stirring solid mixture of **4** (652.3 mg, 0.5 mmol) and KBr (136.7 mg, 1.05 mmol) to afford a brick red suspension. The mixture was stirred at ambient temperature for 3 h and filtered. All volatiles were removed from the red solution, the red residue was washed with pentane (5 ml \times 5) and dried in vacuo to afford **2ThNHRK** as a red solid (385.2 mg, 57%). Single crystals suitable for X-ray diffraction were obtained from benzene solution under ambient temperature. Once obtained as crystalline material, **2ThNHRK** is not soluble in aromatic and aliphatic solvents, and decomposes in coordinative and polar solvents. So, the ¹H and ³¹P NMR spectra were recorded from the NMR scale reaction. However, satisfactory ¹³C and ²⁹Si NMR spectra could not be obtained. The electronic absorption spectrum is also not available for the same reason. Anal. Calcd for C₆₉H₆₉KN₄P₂Si₂Th: C, 61.68; H, 5.18; N, 4.17. Found: C, 59.94; H, 5.25; N, 3.85. ¹H NMR (C₆D₆, 298 K): δ (ppm) 0.11 (s, 18 H, -SiMe₃), 3.93 (s, 1 H, -NHCPh₃), 6.89–7.07 (m, 22 H, ArH), 7.20–7.25 (m, 14 H, ArH), 7.56–7.58 (m, 6 H, ArH), 7.88–7.90 (m, 6 H, ArH). ³¹P NMR (C₆D₆, 298 K): δ (ppm) -2.24 (s). ATR-IR ν cm⁻¹: 3053 (w), 3020 (w), 2946 (w), 2893 (w), 1592 (w), 1483 (m), 1434 (s), 1352 (w), 1244 (s), 1103 (s), 1058 (s), 1025 (s), 893 (s), 828 (s), 749 (s), 697 (s), 633 (m), 594 (m), 546 (m), 523 (s), 510 (m), 480 (s), 414 (m).

Preparation of [Th{C(PPh₂NSiMe₃)₂}(=NCPPh₃)(κ^2 -N, N'-2, 2-bipyridine) (2ThBIPY). At -78 °C, a solution of **2, 2'-BIPY** (0.555 g, 3.55 mmol) and Ph₃CNH₂ (0.922 g, 3.55 mmol) in toluene (20 ml) was added into a stirring toluene solution of **3** (5.705 g, 3.55 mmol, 30 ml) in a dropwise manner. The addition was completed in 1 h. The red solution was allowed to gradually warm to ambient temperature and stirred at ambient temperature for 12 h then filtered. The deep red filtrate was concentrated to approximate 5 ml and stored at -35 °C overnight, affording **2ThBIPY** as a red crystalline solid (2.487 g, 54%). Anal. Calcd for C₆₀H₆₁N₅P₂Si₂Th: C, 59.94; H, 5.11; N, 5.82. Found: C, 60.29; H, 5.02; N, 5.45. ¹H NMR (C₆D₆, 298 K): δ (ppm) -0.04 (s, 18 H, -SiMe₃), 6.87–6.91 (m, 2 H, ArH), 6.93–6.98 (m, 6 H, ArH), 7.02–7.15 (m, 9 H, ArH), 7.20–7.29 (m, 12 H, ArH), 7.40–7.44 (m, 4 H, Pyridine-H), 8.19–8.21 (m, 6 H, ArH), 8.23–8.28 (m, 4 H, Pyridine-H). ³¹P NMR (C₆D₆, 298 K): δ (ppm) -1.26 (s). ¹³C{¹H} NMR (C₆D₆, 298 K): δ (ppm) 3.29 (-SiMe₃), 21.77 (Th = N-CPh₃), 121.70, 124.64, 126.03, 127.46, 128.90, 129.45, 129.67, 130.61 (ArC), 131.91 (t, ²J_{PC} = 6.0 Hz, C_{meta} of P-Ph), 132.15 (t, ²J_{PC} = 6.0 Hz, C_{meta} of P-Ph), 138.22, 139.63, 152.20, 154.33, 156.45 (Pyridine-C). ATR-IR ν cm⁻¹: 3055 (w), 2941 (w), 2894 (w), 1591 (m), 1572 (w), 1478 (m), 1434 (s), 1309 (s), 1242 (s), 1113 (s), 1054 (s), 827 (s), 763 (s), 743 (m), 696 (s), 677 (s), 629 (s), 591 (s), 538 (s), 513 (s), 421 (s).

Preparation of [Th(BIPMTMS)(NHCPPh₃)(CH₂SiMe₃) (5). At -78 °C a solution of Ph₃CNH₂ (136 mg, 0.9 mmol) in toluene (10 ml) was added slowly into a stirring solution of **3** (963.2 mg, 1 mmol) in toluene (10 ml). The mixture was stirred at -78 °C for 15 min, then at ambient temperature for 1 h. The mixture was then filtered, and all volatiles in the yellow filtrate were evaporated under vacuum to afford **5** as a yellow solid. Yield: 0.79 g, 95%. Complex **5** is a thermally unstable complex, decomposing in the solid state in a few days at -35 °C, or in a few hours in C₆D₆ solution at room temperature. Thus reliable microanalyses result, optical, IR, and ¹³C/²⁹Si NMR data are not available. ¹H NMR (C₆D₆, 298 K): δ (ppm)

-0.06 (s, 2 H, -CH₂SiMe₃), 0.04 (s, 18 H, NSiMe₃), 0.49 (s, 9 H, -CH₂SiMe₃), 4.35 (s, 1 H, -NHCPh₃), 6.88–6.93 (m, 6 H, ArH), 7.20–7.26 (m, 9 H, ArH), 7.52–7.55 (m, 9 H, ArH), 7.70–7.81 (m, 6 H, ArH). ³¹P NMR (C₆D₆, 298 K): δ (ppm) 5.49 (s).

Data availability

The X-ray crystallographic coordinates for structures reported in this Article have been deposited at the Cambridge Crystallographic Data Centre (CCDC), under deposition nos. 1861112-1861114. These data can be obtained free of charge from The Cambridge Crystallographic Data Centre (www.ccdc.cam.ac.uk/data_request/cif). All other data can be obtained from the authors on request.

Received: 13 September 2018 Accepted: 15 January 2019

Published online: 07 February 2019

References

- Ephritikhine, M. The vitality of uranium molecular chemistry at the dawn of the XXIst century. *Dalton Trans.* 2501–2516 (2006).
- Kozimor, S. A. et al. Trends in covalency for d- and f-element metallocene dichlorides identified using chlorine K-edge X-ray absorption spectroscopy and time-dependent density functional theory. *J. Am. Chem. Soc.* **131**, 12125–12136 (2009).
- Hayton, T. W. Metal-ligand multiple bonding in uranium: structure and reactivity. *Dalton Trans.* **39**, 1145–1158 (2010).
- Seaman, L. A. et al. Probing the 5f orbital contribution to the bonding in a U(V) ketimide complex. *J. Am. Chem. Soc.* **134**, 4931–4940 (2012).
- Minasian, S. G. et al. Determining relative f and d orbital contributions to M-Cl covalency in MCl₆²⁻ (M = Ti, Zr, Hf, U) and UOCl₅⁻ using Cl K-edge X-ray absorption spectroscopy and time-dependent density functional theory. *J. Am. Chem. Soc.* **134**, 5586–5597 (2012).
- Hayton, T. W. Recent developments in actinide-ligand multiple bonding. *Chem. Commun.* **49**, 2956–2973 (2013).
- Neidig, M. L., Clark, D. L. & Martin, R. L. Covalency in f-element complexes. *Coord. Chem. Rev.* **257**, 394–406 (2013).
- Kaltsayannis, N. Does covalency increase or decrease across the actinide series? Implications for minor actinide partitioning. *Inorg. Chem.* **52**, 3407–3413 (2013).
- Lukens, W. W. et al. Quantifying the σ and π interactions between U(V) f orbitals and halide, alkyl, alkoxide, amide, and ketimide ligands. *J. Am. Chem. Soc.* **135**, 10742–10754 (2013).
- Spencer, L. P. et al. Tetrahalide complexes of the [U(NR)²]²⁺ ion: synthesis, theory, and chlorine K-edge X-ray absorption spectroscopy. *J. Am. Chem. Soc.* **135**, 2279–2290 (2013).
- Polinski, M. J. et al. Unusual structure, bonding and properties in a californium borate. *Nat. Chem.* **6**, 387–392 (2014).
- Jones, M. B. & Gaunt, A. J. Recent developments in synthesis and structural chemistry of nonaqueous actinide complexes. *Chem. Rev.* **113**, 1137–1198 (2013).
- La Pierre, H. S. & Meyer, K. Activation of small molecules by molecular uranium complexes. *Prog. Inorg. Chem.* **58**, 303–416 (2014).
- Liddle, S. T. The renaissance of non-aqueous uranium chemistry. *Angew. Chem. Int. Ed.* **54**, 8604–8641 (2015).
- Cary, S. K. et al. Emergence of californium as the second transitional element in the actinide series. *Nat. Commun.* **6**, 6827 (2015).
- Vitova, T. et al. The role of the 5f valence orbitals of early actinides in chemical bonding. *Nat. Commun.* **8**, 16053 (2017).
- Formanuk, A. et al. Actinide covalency measured by pulsed electron paramagnetic resonance spectroscopy. *Nat. Chem.* **9**, 578–583 (2017).
- Cary, S. K. et al. Incipient class II mixed valency in a plutonium solid-state compound. *Nat. Chem.* **9**, 856–861 (2017).
- Kerridge, A. Quantification of f-element covalency through analysis of the electron density: insights from simulation. *Chem. Commun.* **53**, 6685–6695 (2017).
- Deacon, G. B., Gatehouse, B. M., Shen, Q. & Ward, G. N. Organoamido- and Aryloxo-Lanthanides-VII. The X-ray structure of five-coordinate [La(OC₆H₃Ph₂-2,6)₂(THF)₂](THF). *Polyhedron* **12**, 1289–1294 (1993).
- Cosgriff, J. E., Deacon, G. B. & Gatehouse, B. M. Organoamido- and Aryloxo-Lanthanoids. IX preparations and structures of Tris(η^2 -3,5-diphenylpyrazolato)lanthanoid(III) complexes with triphenylphosphine oxide and tetrahydrofuran. *Aust. J. Chem.* **46**, 1881–1896 (1993).
- Deacon, G. B., Feng, T., Skelton, B. W. & White, A. H. Organoamido- and Aryloxo-Lanthanoids. XI synthesis and crystal structures of Nd(Odpp)₃, Nd(Odpp)₃(thf) and [Nd(Odpp)₃(thf)₂.2(thf) (Odpp⁻ = 2,6-Diphenylphenolate): variations in intramolecular π -Ph-Nd interactions. *Aust. J. Chem.* **48**, 741–756 (1995).

23. Freedman, D., Melman, J. H., Emge, T. J. & Brennan, J. G. Cubane clusters containing lanthanide ions: $(\text{py})_6\text{Yb}_4\text{Se}_4(\text{SePh})_4$ and $(\text{py})_{10}\text{Yb}_6\text{S}_6(\text{SPh})_6$. *Inorg. Chem.* **37**, 4162–4163 (1998).
24. Rabe, G. W., Strissel, C. S., Liable-Sands, L. M., Concolino, T. E. & Rheingold, A. L. Terphenyl ligand systems in lanthanide chemistry: synthesis and structural characterization of two 2,6-dimesitylphenyl derivatives of trivalent Ytterbium. *Inorg. Chem.* **38**, 34463447 (1999).
25. Deacon, G. B., et al. Manipulation of reaction pathways in redox transmetalation-ligand exchange synthesis of lanthanoid(II/III) aryloxide complexes. *Dalton Trans.* 802–812 (2006).
26. Panda, T. K. et al. Imidazol-2-iminato complexes of rare earth metals with very short metal–nitrogen bonds: experimental and theoretical studies. *Inorg. Chem.* **48**, 5462–5472 (2009).
27. Krogh-Jespersen, K., Romanelli, M. D., Melman, J. H., Emge, T. J. & Brennan, J. G. Covalent bonding and the trans influence in lanthanide compounds. *Inorg. Chem.* **49**, 552–560 (2010).
28. Hamidi, S., Deacon, G. B., Junk, P. C. & Neumann, P. Direct reaction of iodine-activated lanthanoid metals with 2,6-diisopropylphenol. *Dalton Trans.* **41**, 3541–3552 (2012).
29. Gholivand, K. & Mahzouni, H. R. Trans influence and covalent bonding in a new octahedral lanthanum(III) complex of diphenylmorpholinyl phosphinamide. *Inorg. Chim. Acta* **386**, 8–12 (2012).
30. Deacon, G. B., Hamidi, S., Junk, P. C., Kelly, R. P., Wang, J. Direct reactions of iodine-activated rare-earth metals with phenols of varying steric bulk. *Eur. J. Inorg. Chem.* 460–468 (2014).
31. Perrin, L., Maron, L. & Eisenstein, O. Some structural and electronic properties of MX_3 ($\text{M} = \text{Ln}, \text{Sc}, \text{Y}, \text{Ti}^+, \text{Zr}^+, \text{Hf}^+$; $\text{X} = \text{H}, \text{Me}, \text{Hal}, \text{NH}_2$) from DFT calculations. *Faraday Discuss.* **124**, 25–39 (2003).
32. Löble, M. W. et al. Covalency in lanthanides. An X-ray absorption spectroscopy and density functional theory study of LnCl_6^{x-} ($x = 3, 2$). *J. Am. Chem. Soc.* **137**, 2506–2523 (2015).
33. La Pierre, H. S. & Meyer, K. Uranium–ligand multiple bonding in uranyl analogues, $[\text{L} = \text{U} = \text{L}]^{n+}$, and the inverse trans influence. *Inorg. Chem.* **52**, 529–539 (2013).
34. Bursten, B. E., Palmer, E. J. & Sonnenberg, J. L. In *Recent Advances in Actinide Science, Special Publications* (eds. May, I., Bryan, N. D. & Alvares, R.) (The Royal Society of Chemistry, London, 2006).
35. Kaltsoyannis, N., Hay, P. J., Li, J., Blaudeau, J.-P. & Bursten, B. E. in *The Chemistry of the Actinide and Transactinide Elements*, 3rd edn. (eds. Morss, L. R., Edelstein, N. & Fuger, J.) pp 1893–2012 (Springer, Dordrecht, 2006).
36. Streitwieser, A. Jr. & Müller-Westerhoff, U. Bis(cyclooctatetraenyl)uranium (uranocene): A new class of sandwich complexes that utilizes atomic f orbitals. *J. Am. Chem. Soc.* **90**, 7364–7374 (1968).
37. Rösch, N. & Streitwieser, A. Jr. Quasirelativistic SCF-Xa scattered-wave study of uranocene, thorocene, and cerocene. *J. Am. Chem. Soc.* **105**, 7237–7240 (1983).
38. Chang, A. H. H. & Pitzer, R. M. Electronic structure and spectra of uranocene. *J. Am. Chem. Soc.* **111**, 2500–2507 (1989).
39. Bursten, B. E., Rhodes, L. F. & Strittmatter, R. J. Bonding in tris(η^5 -cyclopentadienyl) actinide complexes. The ground electronic configurations of “base-free” Cp_3An complexes ($\text{An} = \text{thorium}, \text{protactinium}, \text{uranium}, \text{neptunium}, \text{plutonium}$). *J. Am. Chem. Soc.* **111**, 2756–2758 (1989).
40. Strittmatter, R. J. & Bursten, B. E. Bonding in tris(η^5 -cyclopentadienyl) actinide complexes. A comparison of the bonding in Np, Pu, and transplutonium compounds and with that in lanthanide compounds and a transition-metal analogue. *J. Am. Chem. Soc.* **113**, 552–559 (1991).
41. Li, J. & Bursten, B. E. Electronic structure of cycloheptatrienyl sandwich complexes of actinides: $\text{An}(\eta^7\text{-C}_7\text{H}_7)_2$ ($\text{An} = \text{Th}, \text{Pa}, \text{U}, \text{Np}, \text{Pu}, \text{Am}$). *J. Am. Chem. Soc.* **119**, 9021–9032 (1997).
42. King, D. M. et al. Synthesis and structure of a terminal uranium nitride complex. *Science* **337**, 717–720 (2012).
43. King, D. M. et al. Isolation and characterization of a uranium(VI)–nitride triple bond. *Nat. Chem.* **5**, 482–488 (2013).
44. Tatsumi, K. & Hoffmann, R. Bent $\text{Cis d}^0 \text{MoO}_2^{2+}$ vs. linear $\text{trans d}^0 \text{UO}_2^{2+}$: a significant role for nonvalence 6p orbitals in uranyl. *Inorg. Chem.* **19**, 2656–2658 (1980).
45. Denning, R. G. Electronic structure and bonding in actinyl ions. *Struct. Bond. (Berl.)* **79**, 215–276 (1992).
46. Denning, R. G. Electronic structure and bonding in actinyl ions and their analogs. *J. Phys. Chem. A* **111**, 4125–4143 (2007).
47. Butcher, R. J., Penfold, B. R. & Sinn, E. Crystal structures of *cis*-dibromodioxobis(triphenylphosphine oxide)molybdenum(VI), *cis*-dichlorodioxobis(triphenylphosphine oxide)molybdenum(VI), and *cis*-bis(butane-2,3-diolato)dioxomolybdenum(VI)-butane-2,3-diol (1/2): a comparison of co-ordination spheres and the general stereochemistry of molybdenum(VI) oxo-complexes. *J. Chem. Soc. Dalton Trans.* 668–675 (1979).
48. Bombieri, G., Forsellini, E., Day, J. P. & Azeez, W. I. Crystal and molecular structure of dichlorodioxobis(triphenylphosphine oxide)uranium(VI). *J. Chem. Soc. Dalton Trans.* 677–680 (1978).
49. Vitova, T. et al. Dehydration of the uranyl peroxide studdite, $[\text{UO}_2(\eta^2\text{-O}_2)(\text{H}_2\text{O})_2] \cdot 2\text{H}_2\text{O}$, affords a drastic change in the electronic structure: a combined X-ray spectroscopic and theoretical analysis. *Inorg. Chem.* **57**, 1735–1743 (2018).
50. Dyall, K. G. Bonding and bending in the actinyls. *Mol. Phys.* **96**, 511–518 (1999).
51. Kosog, B., La Pierre, H. S., Heinemann, F. W., Liddle, S. T. & Meyer, K. Synthesis of Uranium(VI) terminal oxo complexes: molecular geometry driven by the inverse trans-influence. *J. Am. Chem. Soc.* **134**, 5284–5289 (2012).
52. Lam, O. P. et al. Observation of the inverse trans influence (ITI) in a uranium (V) imide coordination complex: an experimental study and theoretical evaluation. *Inorg. Chem.* **51**, 6190–6199 (2012).
53. King, D. M. et al. Single-molecule magnetism in a single-ion triamidoamine Uranium(V) terminal mono-oxo complex. *Angew. Chem. Int. Ed.* **52**, 4921–4924 (2013).
54. Lewis, A. J., Carroll, P. J. & Schelter, E. J. Stable Uranium(VI) methyl and acetylde complexes and the elucidation of an inverse trans influence ligand series. *J. Am. Chem. Soc.* **135**, 13185–13192 (2013).
55. Lewis, A. J., Mullane, K. C., Nakamaru-Ogiso, E., Carroll, P. J. & Schelter, E. J. The inverse trans influence in a family of pentavalent uranium complexes. *Inorg. Chem.* **53**, 6944–6953 (2014).
56. La Pierre, H. S. et al. Charge control of the inverse trans-influence. *Chem. Commun.* **51**, 16671–16674 (2015).
57. O’Grady, E. & Kaltsoyannis, N. On the inverse trans influence. Density functional studies of $[\text{MOX}_5]^{n-}$ ($\text{M} = \text{Pa}, n = 2; \text{M} = \text{U}, n = 1; \text{M} = \text{Np}, n = 0; \text{X} = \text{F}, \text{Cl} \text{ or } \text{Br}$). *J. Chem. Soc. Dalton Trans.* 1233–1239 (2002).
58. Kovács, A. & Konings, R. J. M. A theoretical study of the structure and bonding of UOX_4 ($\text{X} = \text{F}, \text{Cl}, \text{Br}, \text{I}$) molecules: the importance of inverse trans influence. *Chemphyschem* **7**, 455–462 (2006).
59. Chermette, H., Rachedi, K. & Volatron, F. Trans effect and inverse trans effect in MLX_5 complexes ($\text{M} = \text{Mo}, \text{U}; \text{L} = \text{O}, \text{S}; \text{X} = \text{Cl}, \text{Br}$): a rationalization within density functional theory study. *THEOCHEM* **762**, 109–121 (2006).
60. Gregson, M. et al. A cerium(IV)–carbon multiple bond. *Angew. Chem. Int. Ed.* **52**, 13016–13019 (2013).
61. Gregson, M. et al. Emergence of comparable covalency in isostructural cerium (IV) and uranium(IV)–carbon multiple bonds. *Chem. Sci.* **7**, 3286–3297 (2016).
62. Gregson, M. et al. The inverse-trans-influence in tetravalent lanthanide and actinide bis(carbene) complexes. *Nat. Commun.* **8**, 14137 (2017).
63. Lu, E., Tuna, F., Lewis, W., Kaltsoyannis, N. & Liddle, S. T. Uranium metallallenes with carbene imido $\text{R}_2\text{C} = \text{U}^{\text{IV}} = \text{NR}'$ Units ($\text{R} = \text{Ph}_2\text{PNSiMe}_3$; $\text{R}' = \text{CPh}_3$): alkali metal-mediated push-pull effects with an amido auxiliary. *Chem. Eur. J.* **22**, 11554–11558 (2016).
64. Lu, E. et al. Uranium-carbene-imido metallallenes: ancillary-ligand-controlled *Cis-/Trans*-isomerisation and assessment of *Trans*-influence in the $\text{R}_2\text{C} = \text{U}^{\text{IV}} = \text{NR}'$ Unit ($\text{R} = \text{Ph}_2\text{PNSiMe}_3$; $\text{R}' = \text{CPh}_3$). *Chem. Eur. J.* **22**, 11559–11563 (2016).
65. Ren, W., Deng, X., Zi, G. & Fang, D.-C. The $\text{Th} = \text{C}$ double bond: an experimental and computational study of thorium poly-carbene complexes. *Dalton Trans.* **40**, 9662–9664 (2011).
66. Scarnborough, C. C. & Wieghardt, K. Electronic structure of 2,2'-bipyridine organotransition-metal complexes. Establishing the ligand oxidation level by density functional theoretical calculations. *Inorg. Chem.* **50**, 9773–9793 (2011).
67. Frisch, M. J. et al. *Gaussian 09, Revision D.01* (Gaussian, Inc., Wallingford, CT, 2016).
68. Perdew, J. P., Burke, K. & Ernzerhof, M. Generalized gradient approximation made simple. *Phys. Rev. Lett.* **77**, 3865–3868 (1996).
69. Perdew, J. P., Burke, K. & Ernzerhof, M. Erratum to generalized gradient approximation made simple. *Phys. Rev. Lett.* **78**, 1396–1396 (1997).
70. Adamo, C. & Barone, V. Toward reliable density functional methods without adjustable parameters: the PBE0 model. *J. Chem. Phys.* **110**, 6158–6170 (1999).
71. Reta, D. et al. The performance of density functional theory for the description of ground and excited state properties of inorganic and organometallic uranium compounds. *J. Organomet. Chem.* **857**, 58–74 (2018).
72. Wu, Q.-Y. et al. Insight into the nature of M–C bonding in the lanthanide/actinide-bis(carbene) complexes: a theoretical perspective. *Dalton Trans.* **47**, 12718–12725 (2018).
73. Glendening, J. K. et al. *NBO 6.0* (Theoretical Chemistry Institute, University of Wisconsin, Madison, 2013).
74. Bader, R. F. W. *Atoms in Molecules: A Quantum Theory* (Oxford University Press, Oxford, 1990).
75. Keith, T. A. *TK Gristmill Software* (Overland Park KS, USA, 2014).

Acknowledgements

We thank the ERC (grant GoG612724), EPSRC (grants EP/P001386/1, EP/M027015, EP/N021932), Marie Curie Incoming Fellowship Scheme (grant 297888), and the University of Manchester for support, and the University of Manchester's Computational Shared Facility for computational resources. We are also grateful to the Pakistan HEC for IRSIP funding to S.S.

Author Contributions

E.L. prepared the compounds and recorded and interpreted the characterisation data. S.S. and V.E.J.B. conducted and interpreted the theoretical calculations. N.K. directed and analysed the computational work and developed the central research idea. A.J.W. collected, solved, and refined the X-ray crystallographic data. S.T.L. originated and developed the central idea, analysed all the data, and wrote the manuscript with contributions from all co-authors.

Additional information

Supplementary Information accompanies this paper at <https://doi.org/10.1038/s41467-019-08553-y>.

Competing interests: The authors declare no competing interests.

Reprints and permission information is available online at <http://npg.nature.com/reprintsandpermissions/>

Journal peer review information: *Nature Communications* thanks Tonya Vitova, Weiqun Shi, and the anonymous reviewer for their contribution to the peer review of this work. Peer reviewer reports are available.

Publisher's note: Springer Nature remains neutral with regard to jurisdictional claims in published maps and institutional affiliations.



Open Access This article is licensed under a Creative Commons Attribution 4.0 International License, which permits use, sharing, adaptation, distribution and reproduction in any medium or format, as long as you give appropriate credit to the original author(s) and the source, provide a link to the Creative Commons license, and indicate if changes were made. The images or other third party material in this article are included in the article's Creative Commons license, unless indicated otherwise in a credit line to the material. If material is not included in the article's Creative Commons license and your intended use is not permitted by statutory regulation or exceeds the permitted use, you will need to obtain permission directly from the copyright holder. To view a copy of this license, visit <http://creativecommons.org/licenses/by/4.0/>.

© The Author(s) 2019